アクティブ運動量交換型衝撃吸収ダンパを用いた衝撃振動制御実験

原　　進*

Experiment of Shock Vibration Control Using Active Momentum Exchange Impact Damper

Susumu HARA

The previous study of the author's group proposed a novel of shock vibration control using the active momentum exchange impact damper (AMEID). By using this method, the shock vibration of the vibratory system is greatly reduced by transferring a part of its momentum to the damper mass. This feature is effective for suppressing the first large peak value of the acceleration response due to a shock load. However, the validity of AMEID for actual implementations has not been investigated yet. In this paper, the active control of shock vibration using AMEID in actual conditions is evaluated by simulation and experiment. A one-degree-of-freedom vibratory system is used as the controlled object. The controller is designed by using the LQR optimal control theory. Reductions of acceleration response and transmitted force to the base are investigated by the simulations. Experiments are carried out to verify the simulation results.

1. INTRODUCTION

Shock vibration has become a common problem in industrial and environmental areas. The large vibration response and transmitted force in forging machines are the examples of shock vibration problems found in industry[1]. These problems decrease machining accuracy and cause vibration pollution to surroundings. Another example of shock vibration problem is floor vibration in multistory buildings due to shock excitation by human activities such as dancing, jumping, etc[2]. This excitation force induces floor vibration and noise to the ceiling of lower rooms. Recently, research on shock and impact problems for mechanical structures, such as conveyance devices and robots, has been increased significantly. For example, Bergés and Bowling discussed the energy based approach to analyze the impact problem in multi-legged robot locomotion[3]. Impacts on a suspension seat have been studied by Wu and Griffin[4].

Several researchers used the tuned mass damper (TMD) method to control shock vibration[5][6]. However, this method can not reduce the maximum peak of the acceleration response.

Some recent studies have discussed shock vibration control induced by collision of two objects. Wang *et al.* utilized the LQI and H_∞ control techniques to control the deformation ratio between two collision objects[7]. To cover the nonlinearity ranges when deformation changes from the elastic range to the plastic range, Wang *et al.* have formulated a linear parameter varying system and applied a gain scheduled (GS) control[8]. Kawashima has proposed a semi-active shock control system in the case that the collision-receiving object has perfect plasticity and the colliding object has perfect elasticity[9]. However, the first large acceleration response can not be decreased by these methods because the shock vibration is reduced by modifying the damping of the system using an actuator.

The passive momentum exchange impact damper

2009年1月14日 受理
* 豊田理化学研究所研究嘱託
(名古屋大学大学院工学研究科)

(PMEID) has been proposed to suppress shock vibration induced by the external excitation force. Different from the previous mentioned methods, in the PMEID, shock vibration of the controlled object is reduced by transferring a part of its momentum to the damper mass. Therefore, the first large acceleration response can be decreased significantly. The application of PMEID to floor shock vibration problems has been proposed[10]. Even though this method effectively reduces both the acceleration response and the transmitted force to the slab, it has one important remaining problem: that the contact parameters should be selected appropriately to obtain optimal damper performance. In actual conditions, the system's operating conditions or parameters change over time. Therefore, the optimal parameters for PMEID drift significantly and its effectiveness is sharply reduced.

Recently, the author's group has proposed an active momentum exchange impact damper (AMEID) for floor shock vibration problem[11]. The simulation results have shown that AMEID has had better performance in comparison with PMEID in reducing the maximum acceleration response of the floor and the transmitted force to the slab. Furthermore, the performance of AMEID does not depend on the system's operating conditions and the contact properties. In addition, AMEID enables us to reduce the size of impact damper mass in comparison with the conventional PMEID. However, the effectiveness of such a control technique for actual implementations has not been addressed yet. Different from our previous paper[11], which utilizes the continuous time controller design for AMEID, this paper utilizes digital controller design. It is very important that the validity of the digital AMEID control is investigated for digital computer based implementations because active shock vibration control is carried out during a very short period. In this paper, the effectiveness in the actual conditions of AMEID is evaluated by simulation. Furthermore, experiments corresponding to the simulation are carried out. By comparing the simulation and the experiment results, it is verified that AMEID is more effective in reducing shock vibration than the previous passive one.

2. DYNAMICAL MODEL

For the experimental study in the following section, a mass supported by a flexible plate is taken as the primary system. The mass is excited by a shock force generated by collisions with a steel ball. The schematic diagram of shock vibration control using AMEID is shown in Fig. 1. It is assumed

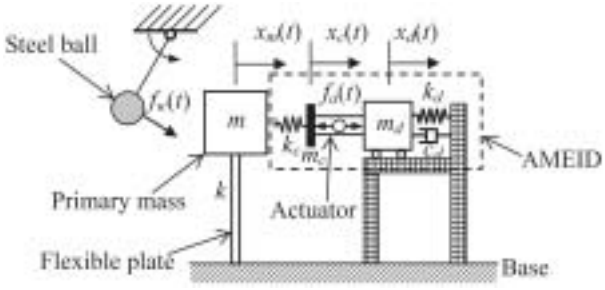

Fig. 1. Dynamic model of AMEID.

that the shock force $f_w(t)$ is given by a half sine function with amplitude F_w and frequency ω_w. The actuator is a voice coil motor installed between the damper mass m_d and the contact spring k_c. It is assumed that the damper mass is supported by a soft spring k_d and a dashpot c_d. The dashpot has a low damping coefficient for forward motion and a high damping coefficient for return motion. When a shock load is applied to the primary mass m, the actuator simultaneously produces an active force $f_a(t) = k_f i_a(t)$, where k_f and $i_a(t)$ are the force constant and the electric current, respectively. This active force pushes the contact spring k_c and the damper mass m_d. As a consequence, the contact spring force increases and compensates the shock load in the primary mass. During the contact period, the contact spring releases its potential energy by transferring a part of its momentum to the damper mass m_d. The governing equations are obtained as follows:

$$m\ddot{x}_m(t)+f_{kc}+kx_m(t)-f_w(t) = 0 \qquad (1)$$

$$m_c\ddot{x}_c(t)-f_{kc}+f_a(t) = 0 \qquad (2)$$

$$m_d\ddot{x}_d(t)+c_d\dot{x}_d(t)+k_dx_d(t)-f_a(t) = 0. \qquad (3)$$

Contact condition between the primary mass and the actuator is modeled using a linear spring. Thus, the contact force can be expressed as:

$$f_{kc} = \begin{cases} k_c[x_m(t)-x_c(t)], & if\ x_m(t) \geq x_c(t) \\ 0, & if\ x_m(t) < x_c(t). \end{cases} \qquad (4)$$

The dashpot c_d has a low damping coefficient c_{dl} for forward and high damping coefficient c_{dh} for return motion as given by

$$c_d = \begin{cases} c_{dl}, & if\ \dot{x}_d(t) \geq 0 \\ c_{dh}, & if\ \dot{x}_d(t) < 0 \end{cases}. \quad (5)$$

The transmitted force to the base is calculated from:

$$f_t(t) = kx_m(t) + c_d\dot{x}_d(t) + k_d x_d(t). \quad (6)$$

The input voltage to the actuator is given by:

$$u_p(t) = k_v[\dot{x}_d(t) - \dot{x}_c(t)] + R_a i_a(t) + L_a \dot{i}_a(t) \quad (7)$$

where k_v, R_a and L_a are the back electromotive force constant, the actuator resistance and the inductance, respectively. The state equation of the analytical model is obtained as follows:

$$\dot{\boldsymbol{x}}_p(t) = \boldsymbol{A}_p \boldsymbol{x}_p(t) + \boldsymbol{b}_b u_p(t) + \boldsymbol{d}_p f_w(t) \quad (8)$$

where
$\boldsymbol{x}_p(t) = [x_m(t)x_d(t)x_c(t)\dot{x}_m(t)\dot{x}_d(t)\dot{x}_c(t)i_a(t)]^{\mathrm{T}}$ and T is the transpose operation.

The actuator of AMEID works only while the contact spring is in contact with the primary mass. During this period, the damping coefficient c_d is assumed to be a constant c_{dl} because the damper mass only moves forward. Therefore, the LQR optimal control theory can be applied to designing the controller of the AMEID. LQR provides a convenient mean of finding feedback gains which produce a stable control system. In many control problems for mechanical structures, the LQR objective functions can be parameterized with relatively few variables so that the control parameters can be tuned easily. For designing the controller we consider the reduced order state equation as follows:

$$\dot{\boldsymbol{x}}(t) = \boldsymbol{A}\boldsymbol{x}(t) + \boldsymbol{b}u(t) + \boldsymbol{d}f_w(t) \quad (9)$$

where $\boldsymbol{x}(t) = [x_m(t)x_d(t)x_c(t)\dot{x}_m(t)\dot{x}_d(t)\dot{x}_c(t)]^{\mathrm{T}}$.

The order of equation (9) is lower than that of equation (8). Equation (9) can be obtained by neglecting the influence of the actuator inductance L_a. In designing the controller for simulations and experiments, the discrete-time model of equation (9) is utilized. However, a more precise model (8) is utilized for the response calculations in the simulations. To implement LQR digital control, the dynamic equation (9) is approximately discretized as:

$$\boldsymbol{A}_d = \exp[\boldsymbol{A}T],\ \boldsymbol{b}_d = \int_0^T \exp[\boldsymbol{A}\tau]d\tau\boldsymbol{b}, \quad (10)$$

where T is the sampling period. The discrete-time state feedback LQR optimal control is obtained by minimizing the criterion function as:

$$J_{LQRD} = \frac{1}{2}\sum_{n=0}^{\infty}[\boldsymbol{x}_d^{\mathrm{T}}(n)\boldsymbol{Q}_d\boldsymbol{x}_d(n) + r_d u_d^2(n)], \quad (11)$$

where n is the sample number, $\boldsymbol{Q}_d =$ diag[q_d 00000] is a symmetric positive-semidefinite matrix and r_d is a positive constant. q_d and r_d are the weights on the primary mass displacement and the control input respectively. Here, we take only the primary mass displacement and the control input as the object functions because the shock vibration of the primary mass and the transmitted force to the base are proportional to the displacement. The feedback control input is given by

$$u_d(n) = -(r_d + \boldsymbol{b}_d^{\mathrm{T}}\boldsymbol{P}_d\boldsymbol{b}_d)^{-1}\boldsymbol{b}_d^{\mathrm{T}}\boldsymbol{P}_d\boldsymbol{A}_d\boldsymbol{x}_d(n) = -\boldsymbol{f}_{bd}\boldsymbol{x}_d(n), \quad (12)$$

where $\boldsymbol{f}_{bd}$ is the discrete-time feedback gain vector and $\boldsymbol{P}_d$ are the positive-definite solutions of the following discrete-time algebraic Riccati equation:

$$\boldsymbol{A}_d^{\mathrm{T}}\boldsymbol{P}_d\boldsymbol{A}_d - \boldsymbol{P}_d - \boldsymbol{A}_d^{\mathrm{T}}\boldsymbol{P}_d\boldsymbol{b}_d(r_d + \boldsymbol{b}_d^{\mathrm{T}}\boldsymbol{P}_d\boldsymbol{b}_d)^{-1}\boldsymbol{b}_d^{\mathrm{T}}\boldsymbol{P}_d\boldsymbol{A}_d + \boldsymbol{Q}_d = \boldsymbol{0}. \quad (13)$$

3. EXPERIMENTAL SETUP

The experimental setup corresponding to Fig. 1 is shown in Fig. 2. The photo of this setup is shown in Fig. 3. The system consists of a primary mass supported by a flexible plate and the voice coil motor as the actuator. The voice coil motor is a direct drive device based on a permanent magnet

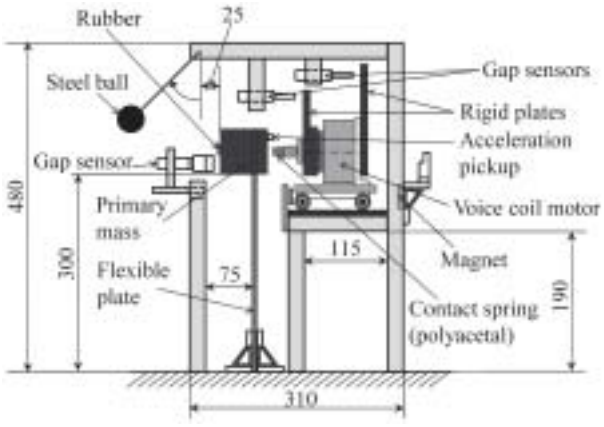

Fig. 2. Schematic diagram of the experimental setup.

Fig. 3. Photo of the experimental setup.

field and current-carrying coil windings. This motor produces a force which is directly proportional to the applied current. In the field of shock vibration control, the main advantage of a voice coil motor is that only the light coil moves, whereas the heavy stator is fixed. The maximum thrust force and stroke of the actuator are 52 N and 5.0 mm, respectively. The stator of the actuator is fixed on an impact damper mass. Therefore, the stator mass is added to the damper mass. The damper mass can move freely in the horizontal direction. The displacement of the primary mass, the actuator coil and the damper mass are detected by the gap sensors. The velocity of the primary mass, the actuator coil and the damper mass are numerically calculated by differentiating the displacements. The acceleration of the primary mass is measured by an acceleration pickup. The shock force is generated by collision of the primary mass with a steel ball. The contact condition between the primary mass and the steel ball is given by a linear spring model. The contact stiffness of the rubber between the primary mass and the steel ball, and the mass of the steel ball are 4.5×10^{3} N/m and 58.8×10^{-2} kg, respectively. The excitation period and the excitation amplitude are 3.5×10^{-2} s and 25 N, respectively.

In the experiment, the signals from the gap sensors and the acceleration pickup are fed to the DSP through analog/digital (A/D) converter, the control input voltage is then calculated. The control input voltage is fed to the power amplifier through the digital/analog (D/A) converter and the amplifier drives the voice coil motor. For the experimental study, as shown in Fig. 3, the impact damper spring k_d and the dashpot c_d are not utilized. This is because the support condition for the impact damper, using a soft spring and one-directional damping, is very difficult to realize in our experimental setup. Therefore, in the simulation, the transmitted force, as given in equation (6), can be written by: $f_t(t) = kx_m(t)$. Even though the transmitted force components: $k_d x_d(t)$ and $c_d \dot{x}_d(t)$ are neglected in this simulation, this simplification has no significant effect because these values are very small in comparison with $kx_m(t)$. The experimental parameters are shown in Table 1. These experimental parameters are used as the nominal parameters. It should be noted that the nominal value for the damper mass ratio (m_d/m) is 1.06.

Table 1. Experimental parameters.

Parameter	Value	Unit
Main mass, m	4.75	kg
Actuator mass, m_c	4.41×10^{-1}	kg
Damper mass, m_d	5.05	kg
Excitation frequency, ω_e	90	rad/s
Excitation amplitude, F_e	25	N
Main spring stiffness, k	2.3×10^{3}	N/m
Damper stiffness, k_d	0.0	N/m
Damping coefficient of the damper, c_d	0.0	Ns/m
Contact stiffness, k_c	2.5×10^{8}	N/m
Actuator inductance, L_c	2.4×10^{-3}	H
Actuator resistance, R_c	3.5	Ω
Back electromotive force constant, k_v	28	Vs/m
Force constant, k_f	28	N/A

4. SIMULATION AND EXPERIMENTAL RESULTS

This section discusses the simulation and experimental studies of the AMEID. At first, the performance of the AMEID due to variation of the system's parameters is investigated by simulation. In this simulation, the numerical calculations of equation (8) are carried out in a MATLAB/Simulink computational environment by using the fourth-order Runge-Kutta method with constant time steps. The controller feedback gains are obtained by the discrete-time LQR control design procedure as explained in the previous section. The discrete-time input voltage to the actuator is calculated from equation (12). Its sampling period is 1.0 ms. Next, experiments are conducted to verify the simulation results.

4.1. The damper mass effect

$q_d = 1.0\times10^8$ and $r_d = 1.0$ are tuned as the nominal values of the LQ control weights. Figure 4 shows the acceleration ratios of the primary mass when the contact stiffness k_c and the impact damper mass ratio m_d/m are varied under the use of the nominal weights controller. It can be seen in Fig. 4

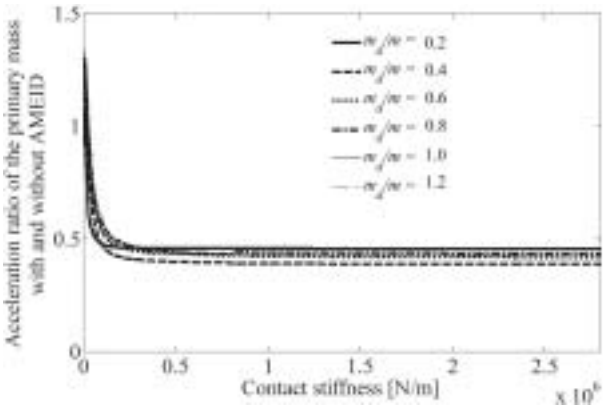

Fig. 4. Relationship between the acceleration ratio with k_c and m_d/m.

that the performance of the AMEID is not much affected by the impact damper mass. It is very important to emphasize that even though a small damper mass has the same effect as a large damper mass, a small damper mass is the most valuable result in this study. However, due to the experimental constraints, we can not reduce the size of the damper mass in the following experimental study.

4.2. Comparison with PMEID

In order to check the effectiveness of the AMEID, its performance is compared with the conventional PMEID as shown in Fig. 5. In this case, the value

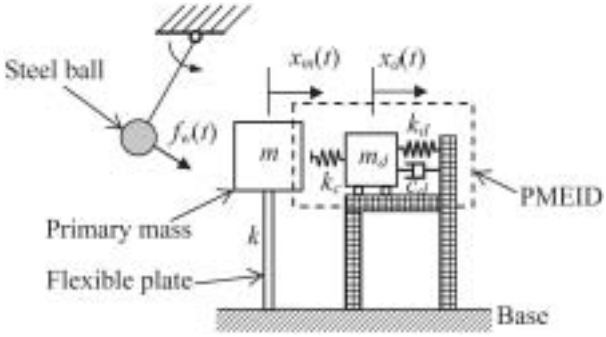

Fig. 5. Schematic diagram of the PMEID.

of contact force is mainly dependent on the impact damper mass m_d and the contact stiffness k_c. As a consequence, the amount of momentum being transferred to the damper mass is very small for small value of m_d. However, in the AMEID case (see Fig. 1), the active force from the actuator simultaneously pushes the contact spring when the shock force exists. Therefore, the reaction force from the contact spring is large and the performance is better than that of the PMEID.

Figure 6 shows the variation of acceleration ratio

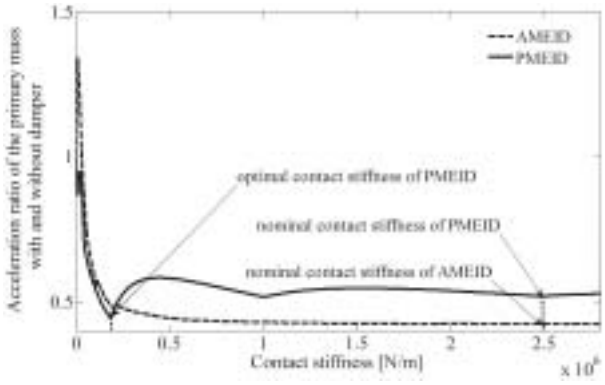

Fig. 6. Relationships between the acceleration ratio and k_c for the AMEID and the PMEIDs.

with contact stiffness k_c using the AMEID and the PMEID. It can be seen in Fig. 6 that the AMEID is better than the PMEID in the wide range of k_c. The PMEID has a very effective point at $k_c = 1.8\times10^5$ N/m theoretically. This contact stiffness is named as the optimal contact stiffness of the PMEID as given by

$$k_{copt} = m_d\omega_w^2\left[\frac{9(9-\beta^2)}{9(\mu+1)-\beta^2}\right], \qquad (14)$$

where β is frequency ratio ω/ω_w, μ is mass ratio m_d/m and $\omega = \sqrt{k/m}$ [12]. Equation (14) shows that the optimal contact stiffness is function of the mass and stiffness of the control system.

For the experimental study, the nominal k_c as shown in Table 1 is used. This is because the optimal contact stiffness k_{copt} is dependent on the system parameters as shown in equation (14). Therefore, it is difficult to realize this contact stiffness in the experiment. It should be noted for the following simulations that the nominal PMEID utilizes the same k_c as used in the experimental study. Meanwhile, the optimal PMEID utilizes k_{copt} as expressed by equation (14).

4.3. Primary mass variation

The numerical comparisons of the maximum acceleration and the maximum acceleration after the shock (residual acceleration) obtained by the AMEID and the PMEID are shown in Fig. 7. In this simulation, the primary mass is varied from the nominal value $0.5 \leq m_{var}/m_{nom} \leq 1.5$. Other parameter values for the PMEID are the same as those of the AMEID. It can be seen in Fig. 7 that the maximum acceleration and the residual acceleration obtained by the AMEID are smaller than those of the PMEID. In addition, the performance of the PMEID decreases when the primary mass is reduced from the nominal value. However, in the AMEID, the performance is not affected by variation of the primary mass.

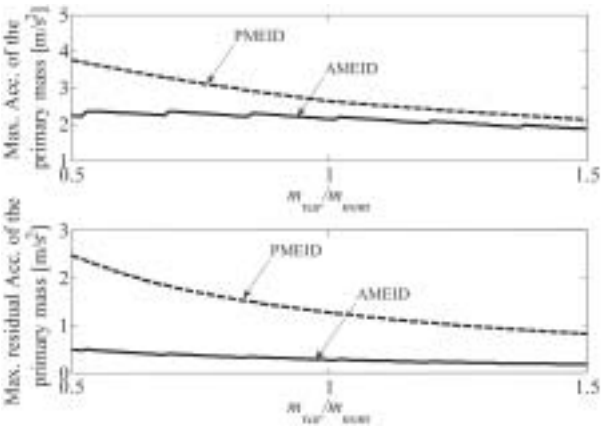

Fig. 7. Maximum acceleration and residual acceleration obtained by the AMEID and the PMEID.

Figure 8 shows the maximum transmitted force obtained by the AMEID and the PMEID when the primary mass is varied. In this simulation, the transmitted force is calculated by: $f_t(t) = kx_m(t)$, because k_d and c_d are zero. As seen in Fig. 8, the maximum transmitted force obtained by the AMEID is smaller than that obtained by the PMEID.

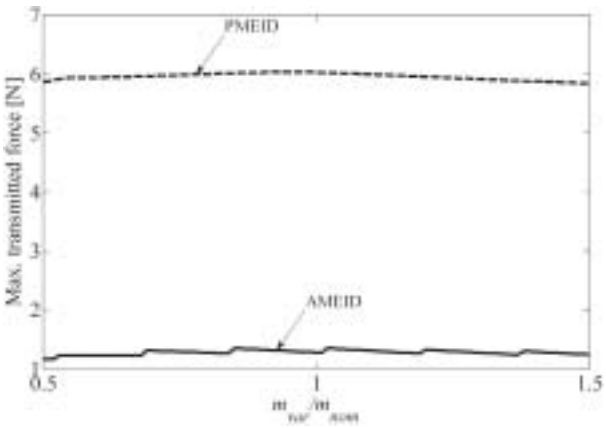

Fig. 8. Maximum transmitted force obtained by the AMEID and the PMEID.

4.4. Shock vibration control experiment

The experimental parameters are shown in Table 1. The initial height of the steel ball before collision with the primary mass is 1.5×10^{-2} m. The maximum value of the excitation force and its contact period are 25 N and 3.5×10^{-2} s, respectively. Due to the experimental constraints, the transmitted force was not measured. However, the primary mass displacement was measured by using a gap sensor. This primary mass displacement is proportional to the transmitted force to the base because k_d and c_d are zero. It is important to note that the square of primary mass displacement (or transmitted force) is proportional to the potential energy of the vibrating system.

The acceleration data obtained by the experiment contain high frequency components. Figure 9 shows an example of the Fourier transform of the acceleration obtained by the experiment without the damper. It can be seen in Fig. 9 that the first natural frequency of the primary mass is about 3.4 Hz. Another peak located at 15.5 Hz is related to the second vibration mode.

For comparison with the simulation data, the acceleration data obtained by the experiment are filtered by a fourth-order low pass filter with 7.0

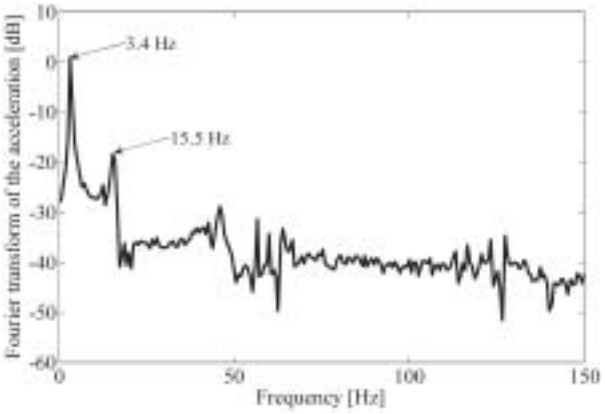

Fig. 9. Fourier transform of the primary mass acceleration.

Hz cut-off frequency. By using this filter, the signal components at frequency higher than the first natural frequency of the flexible plate are removed.

Figure 10 shows the displacement of the primary

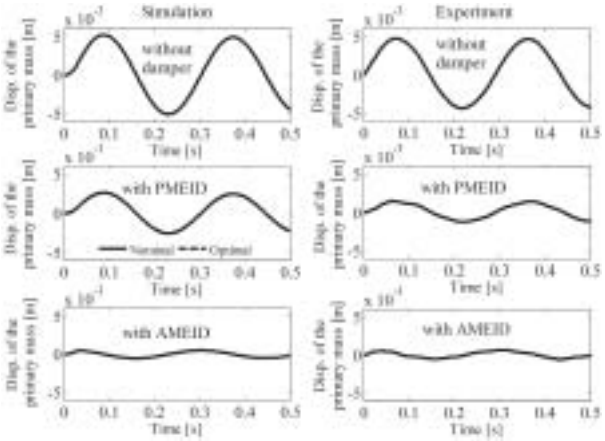

Fig. 10. Displacement of the primary mass.

mass obtained by simulation and experiment for three control cases (i) without damper (ii) with the PMEID and (iii) with the AMEID. In the experiment, the same contact stiffness is used for the PMEID and the AMEID. However, in the simulation study, both the nominal contact stiffness and the optimal contact stiffness are used for the PMEID. It can be seen in Fig. 10 that the maximum displacement responses obtained by the simulation and the experiment agree very well. The experimental results show the maximum displacement of the primary mass could be reduced by 69.2% and 88.7% by using the PMEID and the AMEID, respectively.

Figure 11 shows the acceleration responses of the primary mass obtained by simulation and experiment. In the experiment, the acceleration data are filtered by the low pass filter. Because the shock frequency is higher than the filter cut-off frequency of 7.0 Hz, this filter also removes shock vibration obtained from experimental data as shown in Fig. 11. In the experiment, the maximum residual vibrations are reduced by 70.7% and 78.7% by using the PMEID and the AMEID, respectively.

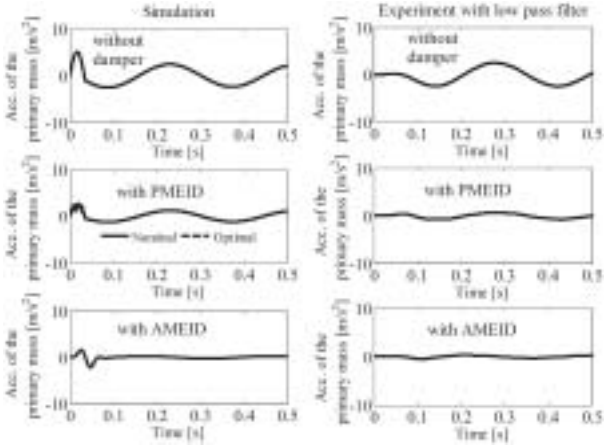

Fig. 11. Acceleration of the primary mass.

The experimental data of the acceleration obtained without and with the low pass filter are compared in Fig. 12. The original data has many

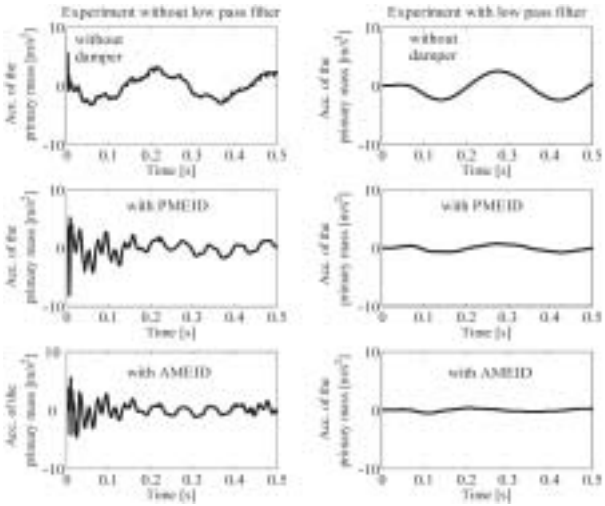

Fig. 12. Acceleration of the primary mass obtained without and with filter.

high frequency components, especially during shock period. In the cases of the PMEID and the AMEID,

the residual vibrations of the first mode are very small. Therefore, the second mode of vibration significantly effects the residual vibration of the acceleration response. In addition, the acceleration response of the experimental result, obtained without the low pass filter, has a very large peak at the initial shock. It is shown in Fig. 12 that the maximum peak obtained by the PMEID is larger than that obtained by the AMEID.

The input voltages of the actuator using the AMEID obtained by the simulation and the experiment are shown in Fig. 13. It can be shown in Fig. 13 that the maximum voltages obtained by the simulation and the experiment agree very well.

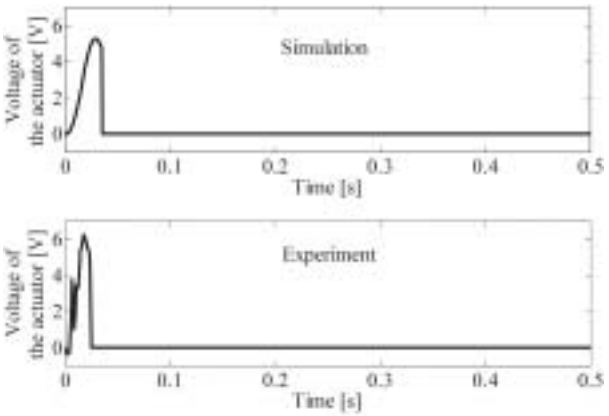

Fig. 13. Voltage of the actuator.

5. CONCLUSION

The purpose of this study is to investigate the effectiveness of the active momentum exchange impact damper (AMEID) for shock vibration control in the actual condition. At first, a control simulation of the AMEID was conducted. The discrete-time LQR optimal control theory was utilized for designing the controller of the AMEID. Simulation results showed that the AMEID is effective in reducing shock vibration. Experiments were carried out to verify the simulation results. It was shown that the experimental results agree well with the results obtained by simulation. Therefore, the effectiveness of the AMEID for actual implementations was verified in this paper.

Acknowledgments

This paper describes the results of collaborative work of the author, Dr. Lovely Son from Andalas University, Indonesia, Dr. Keisuke Yamada from Kyoto University, Japan, and Prof. Hiroshi Matsuhisa from Kyoto University. The author would like to thank for their cooperation. This work was supported by Toyota Physical and Chemical Research Institute, Japan.

REFERENCES

1) N. Tanaka and Y. Kikushima, “A study of a servodamper with preview action (an optimal design for impact vibration control),” *JSME International Journal, Series 3*, **vol. 32**, no. 2, (1989), pp. 215–222.
2) T. Ji and B. R. Ellis, “Floor vibration induced by dance type loads: theory,” *The Structural Engineer*, **vol. 72**, no. 3, (1994), pp. 37–44.
3) P. Bergés and A. Bowling, “Rebound, slip, and compliance in the modeling and analysis of discrete impacts in legged locomotion,” *Journal of Vibration and Control*, **vol. 12**, no. 12, (2006), pp. 1407–1430.
4) X. Wu and M. J. Griffin, “A semi-active control policy to reduce the occurrence and severity of end-stop impacts in a suspension seat with an electrorheological fluid damper,” *Journal of Sound and Vibration*, **vol. 203**, no. 5, (1997), pp. 781–793.
5) M. Setareh and R. D. Hanson, “Tuned mass dampers to control floor vibration from humans,” *ASCE Journal of Structural Engineering*, **vol. 118,** no. 3, (1992), pp. 741–762.
6) A. C. Webster and R. Vaicaitis, “Application of tuned mass dampers to control vibrations of composite-floor systems,” *Engineering Journal of AISC*, **vol. 29**, no. 3, (1992), pp. 116–124.
7) D. Wang, H. Nishimura, and T. Shimogo, “Active control of shock (application of LQI control and H_∞ control),” *Transactions of JSME, Series C* (in Japanese), **vol. 71**, no. 704, (2005), pp. 1223–1230.
8) D. Wang, H. Nishimura, and T. Shimogo, “Active control of shock by gain scheduling,” *Journal of Sound and Vibration*, **vol. 308**, no. 3–5, (2007), pp. 647–659.
9) T. Kawashima, “Consideration of optimal input on semi-active shock control systems (in case of collision-receiving object with plastic property),” *Journal of System Design and Dynamics*, **vol. 2**, no. 1, (2008), pp. 127–138.
10) L. Son, M. Kawachi, H. Matsuhisa, and H. Utsuno, “Reducing floor impact vibration and sound using a momentum exchange impact damper,”

Journal of System Design and Dynamics, **vol. 1**, no. 1, (2007), pp. 14–26.

11) L. Son, K. Yamada, S. Hara, H. Utsuno, and H. Matsuhisa, “Reduction of floor shock vibration by active momentum exchange impact damper,” *Journal of System Design and Dynamics*, **vol. 2**, no. 4, (2008), pp. 930–939.

12) L. Son, “Studies on shock vibration control by momentum exchange impact damper,” *Ph.D. dissertation*, Kyoto University, Japan, (2007).